An Examination of Selected Problems in Rotor Blade Structural Mechanics and Dynamics *

A. Stewart Hopkins
Research Scientist

Robert A. Ormiston
Chief Scientist

Army/NASA Rotorcraft Division, Aeroflightdynamics Directorate (AMRDEC)
US Army Aviation and Missile Command
NASA Ames Research Center, Moffett Field, CA

Abstract

The deformation of rotorcraft blades are frequently classified as moderate, exceeding the small deformation limitation of typical beam finite elements. Advances in computer capabilities have made possible an implementation of a hybrid element combining rigid and flexible body kinematics in the Rotorcraft Comprehensive Analysis System (RCAS). Two challenges to new software are to verify the correctness of the implementation and to ascertain whether it represents an improvement. Comparisons are made to analytical results, to measurements from the "Princeton Beam" and Maryland vacuum chamber experiments, and to UH-60 flight test data. Inspection of these comparisons lead to the conclusion that the results obtained with RCAS correlate well with analytical and experimental results, sometimes representing significant improvements.

Introduction

The broad discipline of rotorcraft dynamics involves a variety of important time dependent and nonlinear phenomena. Even when the major challenges of aerodynamics and material characteristics are ignored, there are many complex fundamental problems involving purely mechanics and structural dynamics phenomena, including rotating systems, large-motion multi-body dynamics, and moderate-to-large deformations of elastic beams of arbitrary shape. In the past these types of problems have often constituted a significant challenge to successful and accurate treatment of important rotorcraft dynamics and aeroelastic phenomena. With the continuing development of advanced comprehensive analysis methods, many of these problems are now amenable to rigorous mathematical treatment and this provides new capabilities for treating many rotorcraft dynamics problems — although not all of the challenges have been reduced to the category of routine engineering.

This paper will examine a number of selected problems relevant to analysis of rotorcraft structural mechanics and dynamics that deal with the issues mentioned above. The focus of this examination will encompass three related themes:

1. a consideration of the methods and philosophy of demonstrating and validating rotorcraft analysis computer programs, and
2. a careful re-examination of a number of important fundamental laboratory experiments,
3. a presentation of results providing initial validation of the RCAS computer program.

This introductory section first provides the background leading to the development of a computer program which implements a hybrid finite element encompassing both rigid and flexible body kinematics. It then describes the implementation of the hybrid element in a computer program. Next, it identifies the methods used for demonstrating and validating the element formulation and software implementation. Finally, it describes the representative problems which were selected for this paper.

This introductory section is followed by four sections of results comparisons. The sections treat groups of problems of the following four types: static elasticity problems, fixed reference frame eigenvalue problems, rotating reference frame eigenvalue problems, and periodic boundary load problems.

Conclusions follow the four results comparison sections.

*Presented at the American Helicopter Society 59th Annual Forum, Phoenix, Arizona, May 6-8, 2003.

Background

The presence of articulated flexible structures such as solar arrays, booms, and antennae on spacecraft stimulated the development of computational methods coupling rigid and flexible body dynamics. Early methods allowed articulated central rigid bodies (typically restricted to a tree topology) with flexible appendages. Ultimately, finite element and modal analysis methods were permitted for the appendages [1].

The governing equations were subsequently reformulated to incorporate rigid body and flexible body degrees of freedom in each body, and to allow arbitrary interconnection topologies [2]. This methodology was incorporated in the General Rotorcraft Aeromechanical Stability Program (GRASP) [3, 4]. GRASP computed eigensolutions for a rotorcraft in vertical flight or ground contact. The run times required to calculate the motion of the reference frame degrees of freedom and the flexible body degrees of freedom associated with each element were high, even on the Cray supercomputer for which it was written.

Using earlier technology, the comprehensive Second Generation Comprehensive Helicopter Analysis System (2GCHAS) [5, 6, 7, 8] ran faster than GRASP, but run times remained a concern. However, it had difficulties with some rigid body motions and moderate deformations. The displacement fields which can be represented by 2GCHAS (and other programs) inadequately represented the combination of rigid body motions of assemblages of elements experiencing moderate deformations.

The Rotorcraft Comprehensive Analysis System (RCAS) [9, 10, 11] is an Army sponsored computer program developed for interdisciplinary engineering, research, and design of arbitrary rotorcraft configurations. Applications include performance, dynamics, aerodynamics, aeroelastic stability, loads and vibration, stability and control, and acoustic characteristics of rotorcraft. RCAS was derived from the Army's previously developed Second Generation Comprehensive Helicopter Analysis System (2GCHAS) and involved significantly changing important parts of the mathematical basis and the system architecture of the 2GCHAS system. These revisions were designed to overcome specific technical limitations of the predecessor 2GCHAS system and have resulted in substantial improvements to the computational efficiency of the system in addition to significantly expanding the functionality and robustness of the system.

Implementation

The principal changes represented in the RCAS mathematical basis and system architecture include a reformulation of the elements that make up the RCAS element library and a revised scheme in which finite elements are assembled into the rotorcraft structure, as described in reference [12]. The new element associates a reference frame a nonlinear beam element with the root of the beam element attached to the origin of the reference frame. Improvements in computer hardware allow rapid calculation of reference frame motion as well as flexible body deformations for every element.

Revised algorithms were required for element assembly. Rather than assembling together all blade nonlinear beam elements referred to a single rotor blade reference frame, the revised approach allows large deformations of the blade while each beam element undergoes only moderate elastic deformations with respect to its own reference frame. Each reference frame is attached to the tip extremity of the adjacent beam element.

An important benefit of the additional reference frames and the revised assembly process is the accuracy and robustness of analyses involving large displacements of the vehicle rigid-body degrees of freedom. In contrast, only a limited capability for large motion maneuvers is available with the basic 2GCHAS formulation. It also makes it feasible to implement a practical modal reduction approach for nonlinear rotor blades that enables significant savings in computational time for typical rotorcraft problems.

Validating Finite Elements

There are two fundamental questions that must be answered when software for a new finite element is developed:

1. Does the software correctly implement the theory for the new element, the assembly of elements, and solution of the resulting equations?
2. Does the new element demonstrate better results than previous elements?

The theory for a finite element is usually derived based on an energy formulation. The types of energy terms involved are elastic energy, kinetic energy (associated both with motion relative to the reference frame and with reference frame motion), and the work done (associated both with body loads and boundary loads).

One way to organize the addressing of the above questions is to answer them for each of the energy terms at the element level. The same questions also need to be answered for the assembly of elements discretizing a continuum (e.g., a blade) and for the heterogeneous assem-

blages of various elements (e.g., a lumped mass) and subassemblies (e.g., a fuselage) which comprise a model.

Some of these questions can be answered through appropriate module testing. But, ultimately, the demonstration and validation must be accomplished by comparison of computed results with known results. There are three types of sources for results:

1. Analytical results are available for some simple configurations. Results may be in closed form, in series form, or in transcendental form with reported solutions. Program results for the configurations it is designed to address should show close agreement.
2. Laboratory experimental results obtained under carefully controlled conditions are available for more complex, but still relatively basic, configurations. Program results should fall within experimental error if systematic apparatus errors are eliminated.
3. Wind tunnel or flight test results are available for real configurations. The complexity of real systems, limited instrumentation, experimental errors due to uncontrolled test conditions, unmodeled features, and uncertainties in system properties are all likely to give rise to discrepancies with program results. However, improvements in correlation here are the acid test of the value of new elements and software.

Selected Problems

Results from a variety of analytical, laboratory and field systems were selected to demonstrate and validate the new element and the RCAS program which implements it. In each case, RCAS was used to solve the computational problem of representing the system and predicting the resulting behavior. RCAS computational results were then compared with the known results for the system. One or more input files specifying the RCAS computational model were written, RCAS was run, and the results were extracted from graphics related files. The representative comparisons presented here are grouped by the finite element energy terms which the problems exercise.

Only elastic energy appears in the first group of problems. Their solutions are static deformations. Comparisons are made to static "Princeton Beam" experiment data and two analytical elastica problems.

The second group of problems adds kinetic energy terms for motion relative to a fixed reference frame. The solutions are natural frequencies. Comparisons are made to dynamic "Princeton Beam" experiment data and an analytical cantilever beam problem.

The third group of problems adds kinetic energy terms associated with a reference frame rotating at a constant angular velocity, including coupling terms (i.e., Coriolis) with motion relative to the reference frame. The solutions are natural frequencies (as a function of rotor speed). Comparisons are made to University of Maryland swept tip beam experiment data and an analytical hinged rotating uniform beam problem.

The fourth group of problems adds the energy terms associated with time varying boundary loading. The solutions are periodic response. Comparisons are made to a full scale rotor, flight-tested extensively during the NASA/Army UH-60 Airloads Program.

Static Elasticity Problems

Three problems tested the elastic energy terms of the element:

1. The analytical problem of a cantilever elastica with a tip moment.
2. The experimental "Princeton Beam" problem of static deflection of a beam with strong, nonlinear edgewise-flatwise-torsion coupling.
3. The analytical problem of a cantilever elastica with a tip load. (The section describing the elastica with tip load problem depends on the "Princeton Beam" section and so is presented after it.)

Elastica with Tip Moment

Helicopter rotor blades, particularly for hingeless and bearingless blades cantilevered to the hub, are typically quite flexible and experience moderately large elastic deformations for which conventional linear beam theory is often inadequate.

The nonlinear beam element formulation is based on the moderate deformation theory of Hodges and Dowell, [13], but the addition of a reference frame attached to the root of each beam element and constrained to move with the tip node of the parent beam element enables arbitrarily large deformation to be accommodated, provided a sufficient number of nonlinear beam elements is employed. The elastica problem comparison with RCAS shows this approach to be very effective, even for beam deflections far beyond those likely to be encountered in rotorcraft applications. The elastica problem, described in many textbooks (e.g., [14]) epitomizes large deflections of beams in two dimensions. Elastica is the name for the shape of elastic curve found from solving the differential equation (Eq. 1) of the deflection curve when the

slopes and deflections become large.

$$EI\frac{d\theta}{ds} = -M \tag{1}$$

Here M is the bending moment, E is the modulus of elasticity, I is the moment of inertia, θ is the angle of rotation of the deflection curve, and s is the distance along the curve.

If the curvature, κ, is constant, it is

$$\kappa = \frac{1}{\rho} = -\frac{M}{EI} \tag{2}$$

With $\theta = 0$ at $s = 0$, the solution is

$$\theta = \kappa s = \frac{1}{\rho}s \tag{3}$$

Here ρ is the radius of curvature. (The theory assumes the beam is thin (its thickness $h << \rho$).)

Selecting a coordinate system, the Cartesian coordinates, r_x, r_y of any point on the deflection curve can be calculated as

$$r_x = \quad \rho\sin\theta \quad = \rho\sin\frac{s}{\rho} \tag{4}$$

$$r_y = \quad \rho(1-\cos\theta) \quad = \rho(1-\cos\frac{s}{\rho}) \tag{5}$$

The RCAS model developed for comparison with this closed form solution was a uniform cantilever beam with a moment applied at the tip. The model had $N = 20$ elements, each of length $l = 1\,\text{ft}$, and an $EI = 9000\,\text{lb/ft}^2$.

Selecting a value of $M = 500\,\text{ft-lb}$ resulted in $\rho = 18\,\text{ft}$. Figure 1 compares the closed form solution (Eqs. 4 and 5) and the solution computed with RCAS for $s = 0\,\text{ft}, \ldots, 20\,\text{ft}$. Note that the maximum angle $\theta = 1.111\,\text{rad} = .3537\pi = 63.66°$.

The results are identical at the figure's resolution. Note that this is for a beam with a tip deflection of about 56% L and a tip slope of about 64°, values far beyond the deflections normally encountered by a rotor blade.

The largest discrepancies in Fig. 1are of the order 6×10^{-4}. Part of the error derives from the numerical methods used to solve the equations. Another portion derives from the element's use of polynomials in contrast to the trigonometric functions in the exact solution. This second form of error, which is intrinsic to the element, can be analyzed, giving insight to the effect of mesh size, N, on accuracy.

For any single element and reasonable mesh size, $s \ll \rho$. (In the above example, $s = L/N = 1\,\text{ft} \ll \rho = 18\,\text{ft}$.) Expanding the sin and cos terms of Eqs. 4 and 5 in a

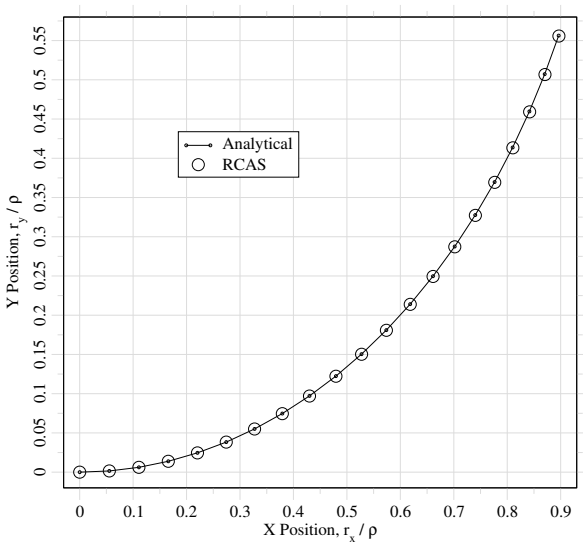

Figure 1: Elastica: analytical vs. RCAS for radius of curvature $\rho = 18\,\text{ft}$ and $L = 20\,\text{ft}$ with $M = 500\,\text{ft-lb}$, $EI = 9000\,\text{lb-ft}^2$, and $N = 20$.

series gives

$$r_x = s(1 - \frac{1}{6}\frac{s^2}{\rho^2} + \frac{1}{120}\frac{s^4}{\rho^4} - \ldots) \tag{6}$$

$$r_y = \frac{s^2}{2\rho}(1 - \frac{1}{12}\frac{s^2}{\rho^2} + \ldots) \tag{7}$$

The expressions used by the element differ slightly. The element's r_x term (which derives from integration of a square root accounting for geometric effects) matches the first two terms in Eq. 6 but differs from the third by being three times as large and opposite in sign. The element's r_y term is the same as the first term in Eq. 7. (This problem has no axial or shear loads so the linear term in r_x and the cubic term in r_y don't appear.) The normalized (by the analytical solution) difference between the element and analytical solutions at the tip of the element can be written (at least for small θ)

$$\varepsilon_x \approx \quad \tfrac{-1}{30}\tfrac{s^4}{\rho^4}|_{s=L/N} = \quad -\frac{L^4}{30\rho^4 N^4} \tag{8}$$

$$\varepsilon_y \approx \quad \tfrac{1}{12}\tfrac{s^2}{\rho^2}|_{s=L/N} = \quad \frac{L^2}{12\rho^2 N^2} \tag{9}$$

For the above example, $L/N = 1\,\text{ft}$ and $\rho = 18\,\text{ft}$, the error predictions are about $\varepsilon_x = -2 \times 10^{-8}$ and $\varepsilon_y = 3 \times 10^{-4}$. The actual numerical differences for the RCAS implementation are $\varepsilon_x = 1 \times 10^{-6}$ and $\varepsilon_y = -2 \times 10^{-3}$

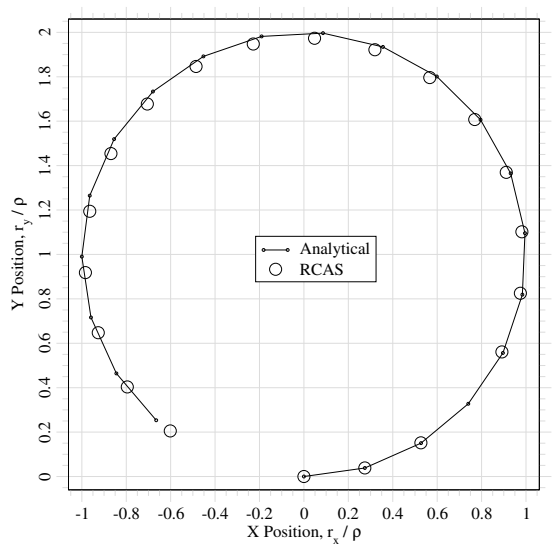

Figure 2: Elastica: analytical vs. RCAS for radius of curvature $\rho = 3.6\,\text{ft}$ and $L = 20\,\text{ft}$ with $M = 2500\,\text{ft-lb}$, $EI = 9000\,\text{lb-ft}^2$, and $N = 20$.

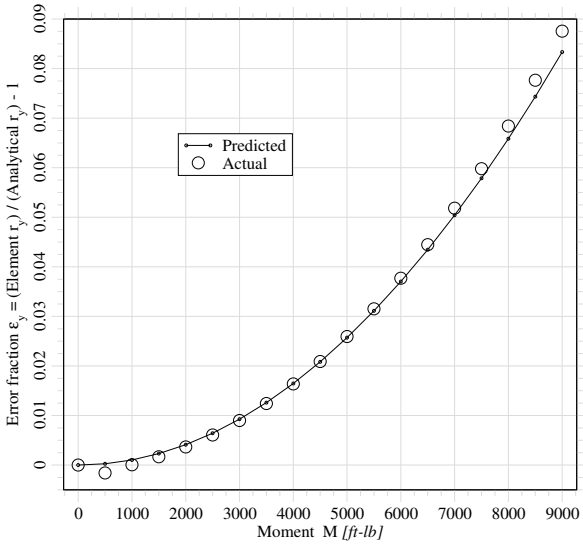

Figure 3: Relative intrinsic element error: predicted vs. actual RCAS error at the end of the first element with $L = 20\,\text{ft}$, $s = 1\,\text{ft}$, $EI = 9000\,\text{lb-ft}^2$, and $N = 20$.

— quite different. Presumably, the numerical errors associated with the solution are larger than the error associated with the element shape functions. This is for a single element, the nonlinear accumulation of errors across N elements is more complex.

The error estimates (Eqs. 8 and 9) suggest the effect of increasing radius of curvature is the same as the effect of increasing number of elements. So the effect of one fifth as many elements on *intrinsic* error is the same as that of quintupling the moment. Selecting a moment of $M = 2500\,\text{ft-lb}$ resulted in $\rho = 3.6\,\text{ft}$. Figure 2 compares the closed form solution and the solution computed with RCAS. Note that in this case the maximum angle $\theta = 5.556\,\text{rad} = 1.768\pi = 318.31°$, which is nearly a full revolution.

For the above example, $L/N = 1\,\text{ft}$ and $\rho = 3.6\,\text{ft}$, the error estimates are $\varepsilon_x = -1.98 \times 10^{-4}$ and $\varepsilon_y = 6.43 \times 10^{-3}$. The actual (RCAS) numerical differences are $\varepsilon_x = -1.94 \times 10^{-4}$ and $\varepsilon_y = 6.07 \times 10^{-3}$ — as predicted. r_y decreases the radius of the elastica. Combined with the more accurate prediction of length this results in an over prediction of θ accumulating to $\theta = 322.86°$, an extra 4.5° at the tip. Surprisingly, the 0.6% error in r_y for a single element when accumulated over $N = 20$ elements leads to a only 1.43% error in θ.

This error comparison, the predicted intrinsic error due to element shape functions vs. the actual error in the RCAS run, is presented for a variety of applied moments in Fig. 3 — noting that relative error shown is:

$$\varepsilon_y = \frac{\text{Actual } r_y - \text{Predicted } r_y}{\text{Predicted } r_y} \tag{10}$$

Note that if the total error includes element intrinsic error and solution error, dividing by the deflection, r_y, amplifies the solution error for small moments (and deflections), explaining the larger discrepancies for small moments.

The actual error is consistent with the expected intrinsic error associated with the shape functions used. Interestingly, the error is less than 9% at $M = 9000\,\text{ft-lb}$ corresponding to a 1 rad rotation in the first element and over three complete revolutions for the $N = 20$ elements.

"Princeton Beam" Static Deformations

The Princeton Beam Problem directly addresses the important nonlinear torsion deflections that accompany the combined edgewise and flatwise bending of a beam. This torsion-bending coupling has important aeroelastic consequences for blade loads and stability. Comparisons between static deformation data from the "Princeton Beam" experiment and RCAS are presented in the next four subsections, which describe the experiment, describe the

RCAS model used, compare horizontal and vertical deflections, and compare twist deflections.

Background

For many years, a standard of comparison for nonlinear beam static and dynamic response has been the "Princeton Beam" experiment. The data provide nonlinear static deformation and natural frequencies for a long slender cantilever beam with a variety of tip weights. Rotating the beam to various angles induced strong nonlinear coupling of edgewise-flatwise-torsion motion. These experiments were performed by E. H. Dowell and J. J. Traybar circa 1974–1975 at the Department of Aerospace and Mechanical Sciences, Princeton University.

Static data from the experiment has been widely used (e.g., [15, 16]), to evaluate nonlinear beam theories — not always with satisfactory results. Note that the first comparisons of the Hodges-Dowell theory with the experiments [15] showed significant deficiencies of the moderate deformation nonlinear beam theory at the largest experimental loading conditions. Rosen and Friedmann [17], using an improved, 3rd-order nonlinear beam formulation showed considerable improvement, but this approach is still subject to the limitations of a theory developed using an ordering scheme. The experiment was carried out in two stages:

1. Dowell and Traybar describe the first stage in [18]. They measured vertical and lateral static deformation of three horizontal, cantilever, slender, rectangular beams, to which they connected a variety of tip masses, while they oriented the beams at a variety of angles. (Due to the rotor blade focus of the experiment, "flap" was used to refer to flatwise motion, "lag" or "chordwise" was used to refer to edgewise motion, "pitch" was used to refer to axial rotation, and "span" or "radius" was used to refer to axial length.) They also measured the first flapwise bending and first lagwise bending frequencies.
2. Dowell and Traybar describe the second stage in [19]. From the beams used in the first experiment, they selected the beam designated # 2 for more accurate measurements of static deformation. They improved the accuracy of their vertical measurements by two orders of magnitude and their lateral measurements by one order of magnitude. In addition to measurements at the tip, they added measurements at intermediate stations. They made additional measurements from which torsional deformation could be estimated. As before, they made these measurements for a variety of tip masses and pitch angles. They did not repeat their frequency measurements.

"Princeton Beam" RCAS Model

The more accurate data from the second experiment were used for comparison. The beam (designated # 2) was of length $R = 20\,\text{in}$, of width $b = 0.5\,\text{in}$, and of height $h = 0.125\,\text{in}$. The beam was machined from 7075-T651 Aluminum alloy, for which the material properties are [20] — density, $\rho = 0.101\,\text{lb/in}^3$; Poisson's ratio, $\nu = .33$; Shear Modulus, $G = 3.9 \times 10^6\,\text{lb/in}^2$; Young's Modulus (averaging the tension and compression moduli), $E = 10.4 \times 10^6\,\text{lb/in}^2$.

The usual formulae were used for cross-section properties ($A = bh$, $I_{flap} = bh^3/12$, $I_{lag} = b^3h/12$). The torsional rigidity, GJ, is a little more challenging. The sometimes erroneously used polar moment of inertia, $J_{polar} = 5.67h^4$ applies to a circular cross-section. The frequently used membrane analogy (e.g., [21]), $J_{membrane} = wh^3/3 = 1.33h^4$ only becomes accurate for larger b/h ratios. For this width to height ratio, $b/h = 4$, Timoshenko and Goodier's result [22] is preferred, $J = 1.124h^4 = 2.744 \times 10^{-4}\,\text{in}^4$.

An RCAS model of the beam was developed with $N = 8$ elements — which the following error analysis suggests as appropriate. The maximum reported flap deformation of the beam was $W = 6.118\,\text{in}$ with a tip load of $P = 3.0\,\text{lb}$ and a pitch angle of $\Theta = -45°$. (The "Princeton Beam" pitch angle, Θ, is measured relative to a vertical chord — so $\Theta = 0°$ corresponds to lagwise loading and $\Theta = \pm 90°$ to flapwise.) The maximum (root) flapwise moment is $M = 3.0\,\text{lb} \times \sin(°{-}45) \times 20\,\text{in}$ which corresponds (Eq. 2) to a radius of curvature $\rho = 19.95\,\text{in}$. Referring to Eq. 9 the anticipated error at the end of the first element is 1.31×10^{-3}. (This estimate is made recognizing that shear and axial loads, non-constant moments and coupling are present, but not accounted for in Eqs. 8 and 9.) Accumulated over the $N = 8$ elements, the intrinsic error would be expected to be of the order 1%.

The early comparisons were quite good — but a systematic pattern was evident in the differences between experimental and RCAS results. The discrepancies tended to be linear in both load and axial station. This pattern is consistent with compliance in the support fixture (a milling machine type, precision, indexing-chuck) or in the root end of the beam. Regression analysis indicated that introducing a root flap hinge with a spring of $26,500\,\text{ft-lb/rad}$ in the RCAS model would eliminate the linear trend in the discrepancies.

"Princeton Beam" Deflections

The experimenters measured vertical deflection (reportedly to $\pm .001\,\text{in}$) and horizontal deflection (reportedly to

$\pm.01$ in). In addition to the tip ($r = R$), measurements were made at $r = R/4$, $r = R/2$, and $r = 3R/4$. They then transformed the measurements to flap deflection, W, and lag deflection, V. It is tempting to make comparisons in these more natural coordinates, but that tends to obfuscate the errors.

The measurements were always made *relative to the unloaded ($P = 0$) condition. Not relative to zero deformation.* In particular, that condition allows deformation of the beam due to its own weight. The running mass amounts to $m \approx 6 \times 10^{-3}$ lb/in or about $1/8$ lb. This can be significant for the smaller loads, especially $P = 1/2$ lb. Accurate comparison requires subtracting the RCAS solution for no tip load ($P = 0$) but including the deformation due to the beam's own weight from the solution with the specified tip load (and the beam's own weight). Deflections of the order $1/8$ in were predicted for the $P = 0$ condition, corresponding to $Z/L = 0.006$, about the size of the larger symbols on the following figures (Figs. 4 and 5).

A comparison of the RCAS and "Princeton Beam" horizontal deflections for a $P = 3.0$ lb tip load is presented in Fig. 4. (Recall the horizontal deflection is flapwise at $\Theta = 0°$ and lagwise at $\Theta = 90°$.) A comparison of the RCAS and "Princeton Beam" vertical deflections for a $P = 3.0$ lb tip load is presented in Fig. 5. (Also recall the vertical deflection is lagwise at $\Theta = 0°$ and flapwise at $\Theta = 90°$.)

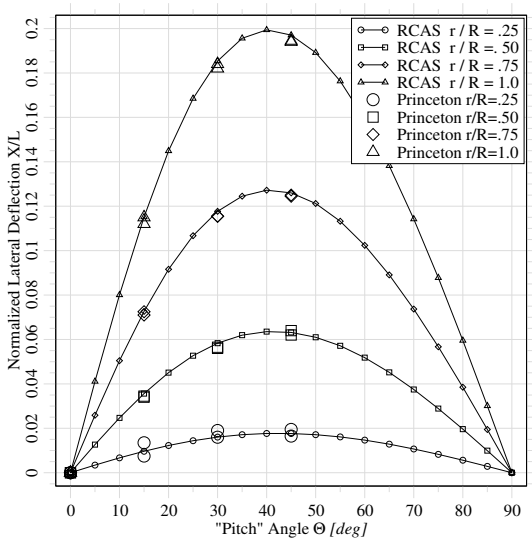

Figure 4: "Princeton Beam" horizontal deflections, X: experiment vs. RCAS for $P = 3.0$ lb and $N = 8$ with $R = 20$ in, $b = 0.5$ in, and $h = 0.125$ in.

"Princeton Beam" Twist

Although there are no applied torsion moments, *per se*, internal torsional moments are an inherent nonlinear consequence of the simultaneous edgewise and flatwise bending. To facilitate twist measurements, the experimenters fastened $L_{rr} = 6$ in reference rods perpendicular to the beam (in the edgewise direction) at $r = R/4$, $R/2$, $3R/4$, and R. In the absence of tip load, the horizontal and vertical distances between the tips of the rods are labeled $X^0_{DISTANCE}$ and $Z^0_{DISTANCE}$. In the presence of tip load, and the resulting elastic twist, the same measurements are labeled $X'_{DISTANCE}$, and $Z'_{DISTANCE}$. With or without load, they are nominally:

$$X_{DISTANCE} \approx 6 \sin\Theta \text{ inches} \quad (11)$$

$$Z_{DISTANCE} \approx 6 \cos\Theta \text{ inches} \quad (12)$$

The experimenters presented twist calculated in two ways — the arc tangent method (better when $\Theta \approx 0°$) and the arc cosine method (better when $\Theta \approx 90°$). The

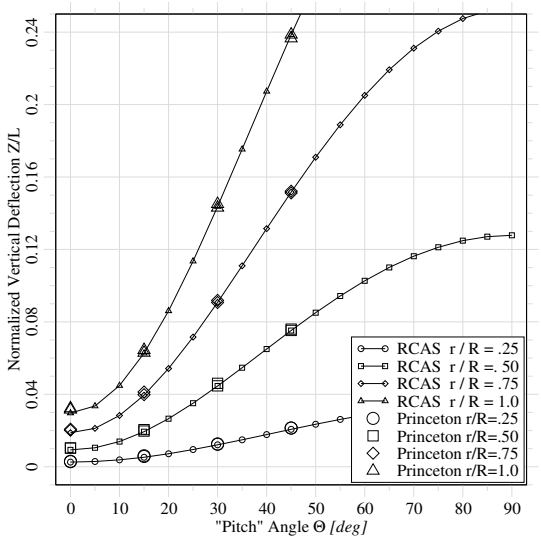

Figure 5: "Princeton Beam" vertical deflections, Z: experiment vs. RCAS for $P = 3.0$ lb and $N = 8$ with $R = 20$ in, $b = 0.5$ in, and $h = 0.125$ in.

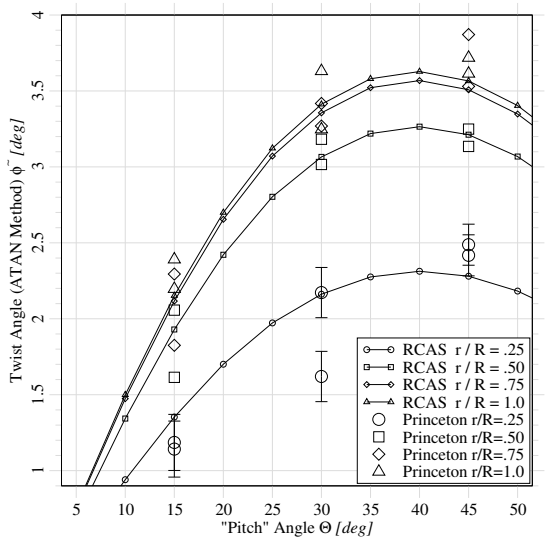

Figure 6: "Princeton Beam" twist angle (arc tangent method), $\tilde{\phi}$: experiment vs. RCAS for $P = 3.0\,\text{lb}$ and $N = 8$ with $R = 20\,\text{in}$, $b = 0.5\,\text{in}$, and $h = 0.125\,\text{in}$.

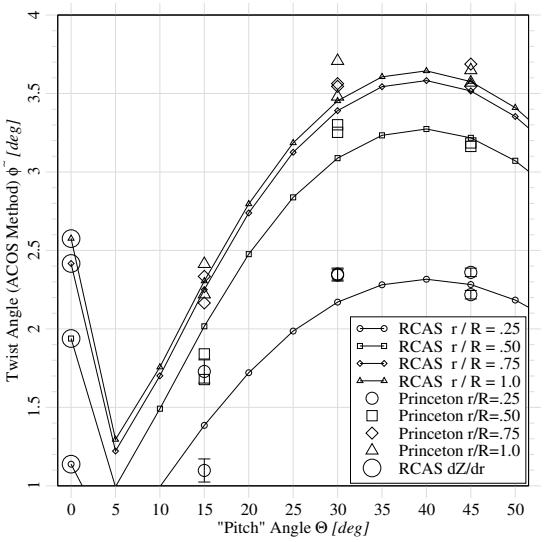

Figure 7: "Princeton Beam" twist angle (arc cosine method), $\tilde{\phi}$: experiment vs. RCAS for $P = 3.0\,\text{lb}$ and $N = 8$ with $R = 20\,\text{in}$, $b = 0.5\,\text{in}$, and $h = 0.125\,\text{in}$.

formulae they presented for the two methods are:

$$\tilde{\phi} = \phi - \phi_0 = \arctan\frac{X'_{DISTANCE}}{Z'_{DISTANCE}} - \arctan\frac{X^0_{DISTANCE}}{Z^0_{DISTANCE}} \tag{13}$$

$$\tilde{\phi} = \phi - \phi_0 = \arccos\frac{Z'_{DISTANCE}}{6.0} - \arccos\frac{Z^0_{DISTANCE}}{6.0} \tag{14}$$

The arc tangent method suffers from a singularity at $Z'_{DISTANCE} = 0$ or $Z^0_{DISTANCE} = 0$, both of which would be expected to occur at $\Theta = 90°$.

Rigid rods were included in the RCAS model equivalent to those in the experiment. The calculations in Eqs. 13 and 14 were carried out using an RCAS calculation for an unloaded beam, $P = 0$, (but, as noted above ("Princeton Beam" Deflections section) not zero deformation due to running mass) to calculate $X^0_{DISTANCE}$ and $Z^0_{DISTANCE}$. A comparison of the results obtained with the arc tangent method, Eq. 13, with the reported results is presented in Fig. 6. Similarly, a comparison of the results obtained with the arc cosine method, Eq. 14, with the reported results is presented in Fig. 7.

One is immediately struck by the apparently spurious results at $\Theta = 0$ using the arc cosine method (Fig. 7). The values are actually a correct result from application of Eq. 14. The projection of the reference rod in the Z direction can be reduced by *either a pitch rotation,* Θ*, or a rotation about the X axis* $\approx dZ/dr$. At $\Theta = 0$, the foreshortening is a result of beam axis bending — not pitch and twist. The slope of the beam axis is plotted on the same figure (Fig. 7).

Given the scatter in the experimental data, it may be instructive to estimate the effect of measurement error on the calculated twist, $\tilde{\phi}$. Assuming the beam is oriented at a twist angle, $\phi \approx \Theta$ or $\phi^0 \approx \Theta$, and that there are unknown measurement errors, $\varepsilon_{x'}$ and $\varepsilon_{z'}$ or ε_{x^0} and ε_{z^0}, equations Eqs. 13 and 14, with Eqs. 11 and 12 give:

$$\tilde{\phi} \approx \arctan\frac{6\sin\phi + \varepsilon_{x'}}{6\cos\phi + \varepsilon_{z'}} - \arctan\frac{6\sin\phi_0 + \varepsilon_{x^0}}{6\cos\phi_0 + \varepsilon_{z^0}} \tag{15}$$

$$\tilde{\phi} \approx \arccos\frac{6\cos\phi + \varepsilon_{z'}}{6.0} - \arccos\frac{6\cos\phi_0 + \varepsilon_{z^0}}{6.0} \tag{16}$$

Noting the derivatives:

$$\frac{\partial}{\partial x}\arctan\frac{6\sin\phi + x}{6\cos\phi} = \frac{\cos\phi}{6} \tag{17}$$

$$\frac{\partial}{\partial x}\arccos\frac{6\cos\phi + x}{6.0} = \frac{-1}{6\sin\phi} \tag{18}$$

Neglecting ε_z in comparison to ε_x, the errors in the two calculations are:

$$\varepsilon_{\tilde{\phi}} \approx \frac{\cos\Theta}{6}\varepsilon_{x'} - \frac{\cos\Theta}{6}\varepsilon_{x^0} \tag{19}$$

$$\varepsilon_{\tilde{\phi}} \approx \frac{-1}{6\sin\Theta}\varepsilon_{z'} - \frac{-1}{6\sin\Theta}\varepsilon_{z^0} \tag{20}$$

For $\Theta = 15°$, 30°, and 45°, the sensitivities are about 9°/in, 8°/in, 7°/in, respectively, for the arc tangent method; and 37°/in, 19°/in, 14°/in, respectively, for the arc cosine method. The experimenters reporting measurement accuracies of $\pm.01$ in laterally, and $\pm.001$ in vertically. The statistical combination of the errors in the eight measurements (two for $X^0_{DISTANCE}, \ldots$) multiplied by the sensitivities yield about $\pm 0.18°$, $\pm 0.16°$, and $\pm 0.14°$ for the arc tangent method and $\pm 0.07°$, $\pm 0.04°$, and $\pm 0.03°$ for the arc cosine method at $\Theta = 15°$, 30°, and 45°, respectively.

To limit the clutter, these error estimates are illustrated in Figs. 6 and 7 for only station $r/R = 0.25$. For each angle, Θ, the size of the error bar is the same at all stations. The data scatter using the arc tangent method is consistent with the predicted error estimates and the reported measurement error; the scatter using the arc cosine method is less so.

Since the reported calculations seem to obscure the comparison, the calculation was inverted. Assuming Eqs. 11 and 12 are exact (instead of approximate when $X_{DISTANCE}$ is replaced with $X^0_{DISTANCE}$ (and $Z_{DISTANCE}$ with $Z^0_{DISTANCE}$), Eqs. 13 and 14 can be solved for $X'_{DISTANCE}$ and $Z'_{DISTANCE}$. Calculating the difference between the measurement and the nominal values (Eqs. 11 and 12) and normalizing by the length of the reference rod, $L_{rr} = 6$ in, the twist related measurement is compared with the same calculation using RCAS results in Figs. 8 and 9.

Again, to limit the clutter, these error estimates are illustrated in Figs. 8 and 9 for only station $r/R = 0.25$. For each angle, Θ, the size of the error bar is the same at all stations. The "Princeton Beam" data, the error bounds and the RCAS results are all reasonably consistent.

Elastica with Tip Load

Another problem for which an analytical solution exists is the tip loaded elastica. The solution is in the form of a transcendental equation involving elliptic functions. Solutions are available from a variety of sources — those from reference [14] are used for comparison here. Normalized elastica angle of rotation, $\theta_b/\frac{\pi}{2}$, vertical deflection, δ_v/L, and horizontal deflection, δ_h/L (all at the tip) vs. normalized loads, PL^2/EI, are tabulated op. cit. for a cantilever beam of length L, modulus of elasticity E, and moment of inertia I, subjected to a (downward) tip load P. Note that horizontal deflection, δ_h for this problem refers to the shortening of the projection of the beam axis in the axial direction, *not* lateral deflection as with the "Princeton Beam".)

The RCAS model developed for the "Princeton Beam"

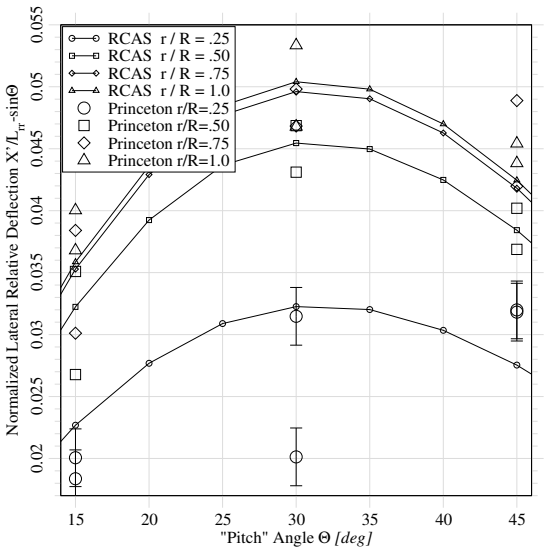

Figure 8: "Princeton Beam" twist: normalized relative lateral deflection, $X'/L_{rr} - sin\Theta$: experiment vs. RCAS for $P = 3.0$ lb and $N = 8$ with $R = 20$ in, $b = 0.5$ in, and $h = 0.125$ in.

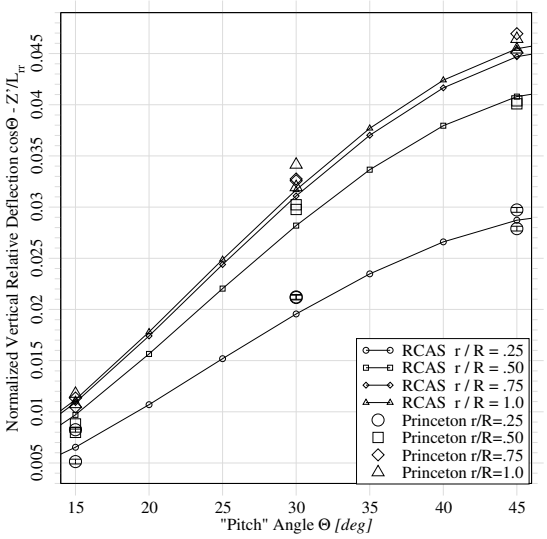

Figure 9: "Princeton Beam" twist: normalized relative vertical deflection, $cos\Theta - Z'/L_{rr}$: experiment vs. RCAS for $P = 3.0$ lb and $N = 8$ with $R = 20$ in, $b = 0.5$ in, and $h = 0.125$ in.

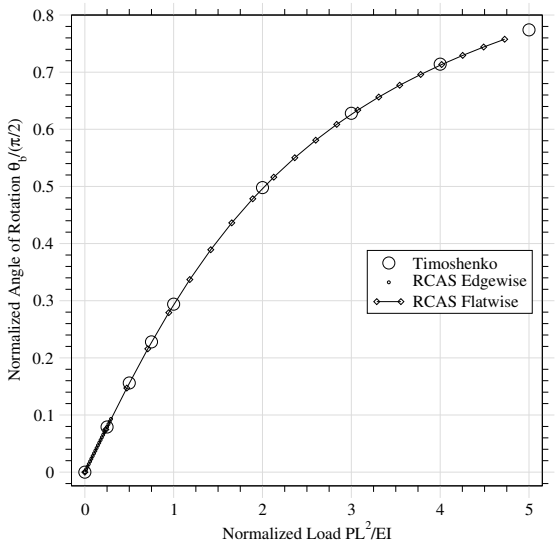

Figure 10: Tip Loaded Elastica: Rotation Angle, θ_b vs. RCAS for $L = 20\,\text{in}$, $N = 8$, $P = 0.5 \ldots 10\,\text{lb}$ and $EI = 8.463 \times 10^2$ or $1.354 \times 10^4\,\text{lb/in}^2$.

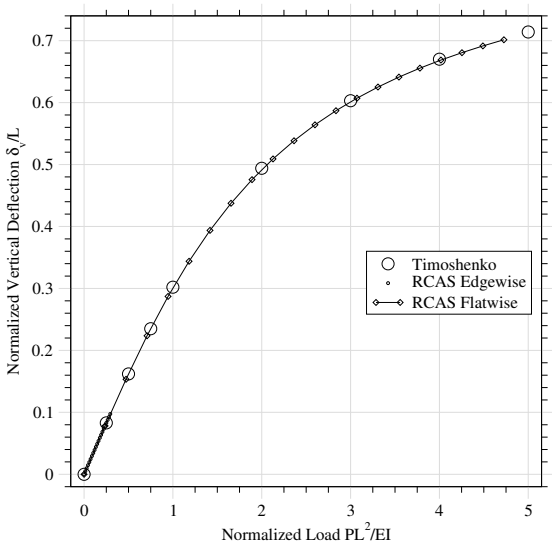

Figure 11: Tip Loaded Elastica: Vertical Displacement, δ_v vs. RCAS for $L = 20\,\text{in}$, $N = 8$, $P = 0.5 \ldots 10\,\text{lb}$ and $EI = 8.463 \times 10^2$ or $1.354 \times 10^4\,\text{lb/in}^2$.

comparison, discussed above, was reused since it allowed direct comparison to the experimental results. The flap hinge and spring (which modeled root compliance) was the only feature removed. In particular, shear and axial deflections were allowed but were expected to be negligible. Running mass was retained, although, as discussed previously ("Princeton Beam" Deflections section) the unloaded solution ($P = 0$) was subtracted from the RCAS solutions. This model only approximated the analytical problem, so exact comparison was not anticipated.

Restricting this $N = 8$ element, $L = 20\,\text{in}$ model to $\Theta = 0°$ and 90° eliminated the edgewise-flatwise-torsion coupling. At 0°, the bending is lagwise with $EI = 1.354 \times 10^4\,\text{lb/in}^2$ and at 90°, the bending is flapwise with $EI = 8.464 \times 10^2\,\text{lb/in}^2$.

The RCAS model was run for tip loads of $P = 0.5, \ldots, 10\,\text{lb}$ corresponding to normalized loads of 0.24-4.7 flapwise and 0.015-0.30 edgewise. A comparison of analytical and RCAS results is presented in Fig. 10 for normalized tip bending rotation, Fig. 11 for normalized vertical displacement, and Fig. 12 for normalized axial displacement. At the largest load, $P = 10\,\text{lb}$, the beam tip angle is $\theta_b \approx 68°$, the vertical displacement is $\delta_v \approx 14\,\text{in} = .7L$, and the horizontal displacement is $\delta_v \approx 7.6\,\text{in} = .38L$.

The RCAS edgewise data points only appear as a thickening of the line in the lower left corner of each

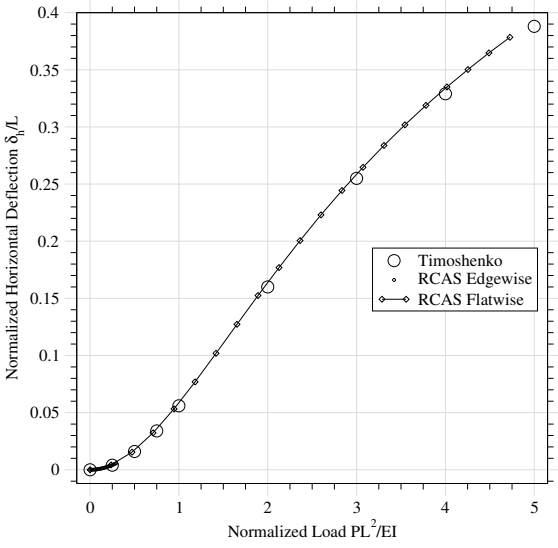

Figure 12: Tip Loaded Elastica: Horizontal Displacement, δ_h vs. RCAS for $L = 20\,\text{in}$, $N = 8$, $P = 0.5 \ldots 10\,\text{lb}$ and $EI = 8.463 \times 10^2$ or $1.354 \times 10^4\,\text{lb/in}^2$.

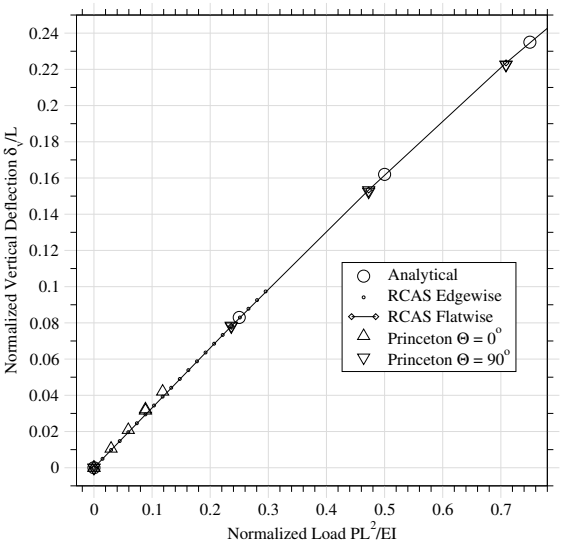

Figure 13: Tip Loaded Elastica: Vertical Displacement, δ_v vs. RCAS and vs. "Princeton Beam" for $L = 20\,\text{in}$, $N = 8$, $P = 0.5 \ldots 10\,\text{lb}$ and $EI = 8.463 \times 10^2$ or $1.354 \times 10^4\,\text{lb/in}^2$.

graph. The data from the "Princeton Beam" experiment are superimposed on Fig. 11 and presented at a magnified scale in Fig. 13.

The analytical, "Princeton Beam", and RCAS results are quite consistent, confirming the expectations that shear and axial deformation were negligible. It also supports the expectation that

Fixed Frame Dynamics Problems

Two problems tested the kinetic energy terms of the element for motion relative to a fixed reference frame:

1. The experimental "Princeton Beam" problem of frequencies at static equilibrium of a beam with strong, nonlinear edgewise-flatwise-torsion coupling.
2. The analytical problem of the eigenvalues of a cantilever beam.

"Princeton Beam" Frequencies

As previously noted ("Princeton Beam" Static Deformations section), frequency data was gathered during the "Princeton Beam" experiment, although previous investigators have made very little use of this data. These measurements provide the first flapwise and chordwise natural frequencies for vibrations in the presence of the substantial edgewise-flatwise-torsion static deformations discussed above.

For the static measurements, the experimenters suspended a weight pan by a thread connected to a screw in the end of the beam and added weights to produce the desired static load. They had to use a different approach for dynamics. Judging from a photo and a drawing, they machined a hollow cylindrical mass with a central web, which was slid over the end of the beam and fastened, through the web, to the end of the beam. The mass shown was of length about $3/4$ of the diameter. Other than the photo and drawing, no information was available regarding the dimensions of the weights.

To provide a rough estimate of rotary inertia, the inertia was assumed to be that of a hollow cylinder ($I_{xx} = I_{zz} = m(3R^2 + 3r^2 + h^2)/12$) of the specified weight and of the same 7075-T651 Aluminum alloy. The mass and volume are thus $m = P/g = \rho V$. The length was assumed to be $h = 1.5\sqrt{3}V/(1.5\pi)$. The inner radius was taken to be $r = .025\,\text{ft}$. The outer radius was then calculated as $\sqrt{V/(\pi h) + r^2}$. The result is a hollow cylinder, of the correct weight, large enough to fit over the beam with a little clearance, and whose length ($h \approx 1.5R$) is within a few percent of $3/4$ of the outer diameter.

A comparison of "Princeton beam" experimental and RCAS results is presented in Fig. 14 for tip masses weighing $P = 2\,\text{lb}$ and $P = 3\,\text{lb}$. Figure 15 presents the flapwise results at a different scale. The results show the effect of static equilibrium deflections of the beam on the natural frequencies as well as the nonlinear coupling due to the combined bending and torsion for the non-zero pitch angles. The quite acceptable agreement validates the theoretical basis of RCAS.

Cantilever Beam Frequency Comparisons

In the absence of a tip mass, the results from the previous ("Princeton Beam" Frequencies section) admit an analytical solution. Many textbooks (e.g., [23]) provide the natural frequencies for a uniform cantilever beam as:

$$\omega_n = (\beta l)_n^2 \sqrt{\frac{EI}{ml^4}} \tag{21}$$

where $(\beta l)_1 \approx 1.875$ is the reported solution to the transcendental equation for the first natural frequency.

The analytical solution (using the RCAS value for gravity, $g = 32.17405\,\text{ft/sec}^2$ to calculate mass), the "Princeton Beam" experimental frequencies, and the frequencies RCAS calculated for the same conditions ($\Theta = 0°$ or $90°$ and $P = 0$ are tabulated for the first flatwise and first edgewise frequencies in Table 1.

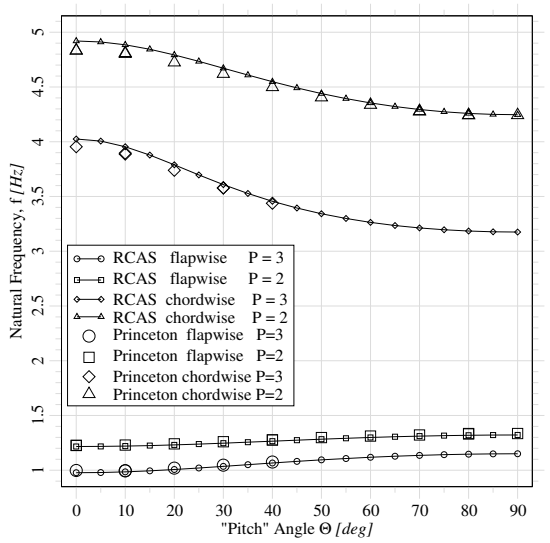

Figure 14: "Princeton Beam" natural frequencies of first flapwise and chordwise modes: experiment vs. RCAS for $P = 2\,\text{lb}$ and $P = 3\,\text{lb}$ and $N = 8$ with $R = 20\,\text{in}$, $b = 0.5\,\text{in}$, and $h = 0.125\,\text{in}$.

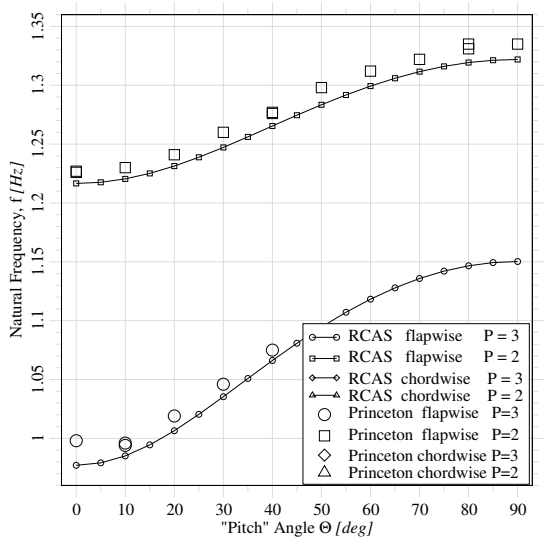

Figure 15: "Princeton Beam" natural frequencies of first flapwise mode: experiment vs. RCAS for $P = 2\,\text{lb}$ and $P = 3\,\text{lb}$ and $N = 8$ with $R = 20\,\text{in}$, $b = 0.5\,\text{in}$, and $h = 0.125\,\text{in}$.

Cantilever Beam Natural Frequencies		
Model	Flatwise	Edgewise
Analytical	10.0642	40.2570
RCAS $\Theta = 0°$	10.0605	40.0719
RCAS $\Theta = 90°$	10.0602	40.0748
Princeton $\Theta = 0°$	10.154 10.152 10.143	41.143

Table 1: Cantilever beam natural frequencies: analytical vs. RCAS vs. "Princeton Beam" for $N = 8$ with $R = 20\,\text{in}$, $b = 0.5\,\text{in}$, and $h = 0.125\,\text{in}$.

Rotating Frame Dynamics Problems

Two problems tested the kinetic energy terms of the element for motion relative to a reference frame rotating at a constant angular velocity:

1. The experimental frequencies of a swept tip, rotating beam, measured in the University of Maryland vacuum chamber.
2. The analytical problem of the natural frequencies of a hinged rotating beam.

University of Maryland Rotating Beam Frequencies

Comparisons between natural frequency data from a University of Maryland swept tip beam experiment and RCAS are presented in the next three subsections. The experiment is described, the RCAS model is described and comparisons of natural frequencies are presented.

Swept Tip Background

The effect of blade tip sweep angle on rotor blade structural dynamics was a nontrivial problem for rotorcraft when such blades were introduced for aerodynamic and aeroelastic reasons. Celi and Friedmann [24] provided one of the first satisfactory treatments of the problem although good experimental data for fundamental validation swept tip blade frequencies was scarce until rotating blade data was obtained in the University of Maryland vacuum chamber. This set of experimental data was obtained by the Department of Aerospace Engineering at the University of Maryland. The "University of Maryland" data [25] provides *in vacuo*, rotating frequencies of a blade with the outboard 16% swept at various angles. Although the experiment included composite as well as aluminum blades, only the results obtained with the aluminum blade are used for comparison.

The geometry is slightly more complex than the problems discussed above. The experimenters used uniform, untwisted rotating beams with a 16%, 0° to 45° swept tip. They were spin tested in the University of Maryland vacuum chamber.

Experimental frequency measurements have been compared with a finite element analysis by Epps and Chandra [25] as well as with a more accurate theory by Hodges, Shang, and Cesnick [26]. Although these theories were reasonably successful, neither study included static gravity deflections and there has been some confusion about the modal content of the analytical and experimental results. In both papers, [25, 26], frequencies are plotted as a function of sweep angle at the test angular velocities.

The experimental data used for the comparison described below was scaled from the figures in [25]. The data was for what was labeled the first five flap modes and the first torsion mode. The rotor speeds presented were for 0, 500, and 750 RPM. The tested beams had sweep angles of 0°, 15°, 30°, and 45°.

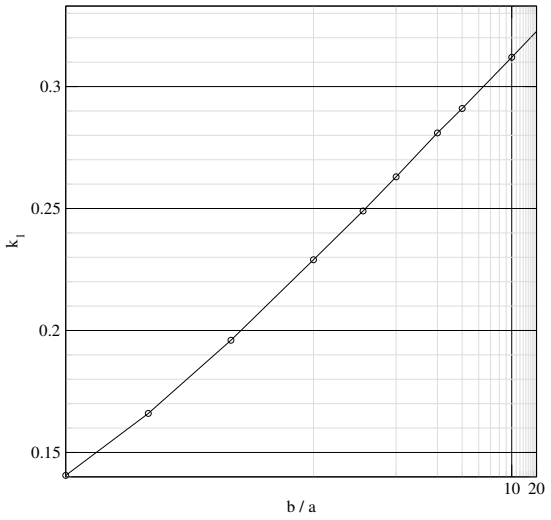

Figure 16: Reciprocal Scale Plot of Constants for Torsion of a Rectangular bar from Timoshenko and Goodier [22].

Swept Tip RCAS Model

The unswept rotor radius was $R = 40\,\text{in}$, which included a hub of radius $r_{hub} = 2.5\,\text{in} = .0625R$, a beam of length $r_{swp} - r_{hub} = 31.5\,\text{in} = .7875R$, and a tip section of length $r_{tip} - r_{swp} = 6\,\text{in} = .15R$. Both the beam section and the tip section were of width $b = 1.0\,\text{in}$, and of height $h = 0.063\,\text{in}$. The aluminum alloy is not specified in the paper, so it was assumed to be 7075 with the previously noted ("Princeton Beam" RCAS Model section) material properties and cross-section formulae.

Again, torsional rigidity is more challenging. This width to height ratio, $b/a = 1/0.063 = 15.873$, is not tabulated in references such as Timoshenko and Goodier [22]. However, if the tabulated values are plotted with an reciprocal scale (Fig. 16), a value of $\kappa_1 = .320$ can be inferred. The corresponding $J = \kappa_1 h^3 b = 8.0015 \times 10^{-5}\,\text{in}^4$.

An RCAS model of the beam was developed with $N = 14$ elements to represent the beam section and $N = 3$ elements to represent the tip.

Swept Tip Frequency Comparisons

Each figure in the papers [25, 26] presented experimental data and theoretical curves for a single mode's frequency as a function of sweep angle at the three rotor speeds. The experimenters presented six figures which they labeled flap modes 1–5 and torsion. All experimental data presented here is labeled according to their definitions.

The interpretation of the modal frequency variations with blade tip sweep angle, Λ, and with rotor speed, Ω, are facilitated by comparing frequency vs. sweep angle and frequency vs. rotor speed fan plots. A comparison of non-rotating ($\Omega = 0$) RCAS frequencies vs. experimental data, without gravity is presented in Fig. 17. A comparison of unswept ($\Lambda = 0$) RCAS frequencies vs. experimental data, without gravity is presented in Fig. 18.

The first eight flap modes are easily identified. The first torsion and the first two lag modes are also clear, showing very little increase with frequency due to centrifugal stiffening. The RCAS frequencies are identified as f1–f4 and f8 for the first four and eighth flap modes; l1 and l2 for the first two lag modes; c1–c3 for three coupled modes which at $\Lambda = 0$ and $\Omega = 0$ are the fifth through seventh flap modes; and c4 for the fourth coupled mode, which at $\Lambda = 0$ and $\Omega = 0$ is the first torsion mode.

When gravity is included in the RCAS calculations, the non-rotating and unswept frequencies are shown in Figs. 19 and 20. The effects of gravity are significant only at the lowest rotor speeds, as would be expected with a centripetal acceleration of nearly 640 g at the tip for Ω_{nom} dominating the acceleration of gravity at other rotor speeds. At the lowest rotor speeds, the weight of the blade results in flapwise or primarily flapwise (when $\Lambda \neq 0$) static deflection. This static deflection has only a small effect on the blade flap frequencies. However,

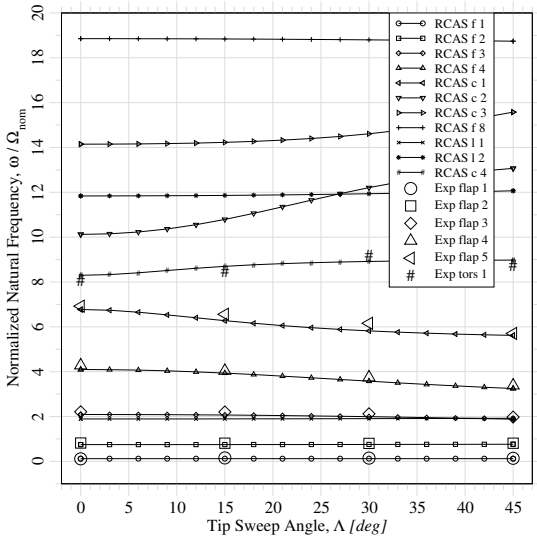

Figure 17: Swept tip natural frequencies: experiment vs. RCAS for $N = 17$ and $\Omega = 0$ with *no* gravity.

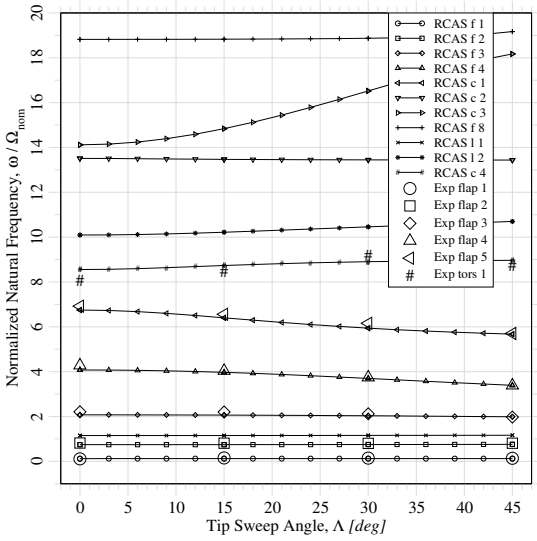

Figure 19: Swept tip natural frequencies: experiment vs. RCAS for $N = 17$ and $\Omega = 0$ with gravity.

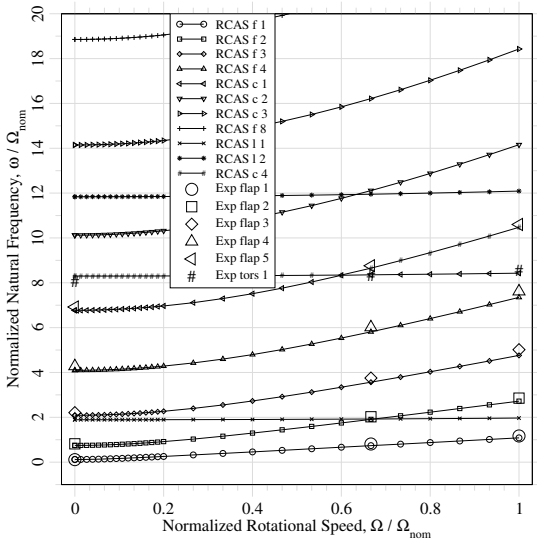

Figure 18: Swept tip natural frequencies: experiment vs. RCAS for $N = 17$ and $\Lambda = 0°$ with *no* gravity.

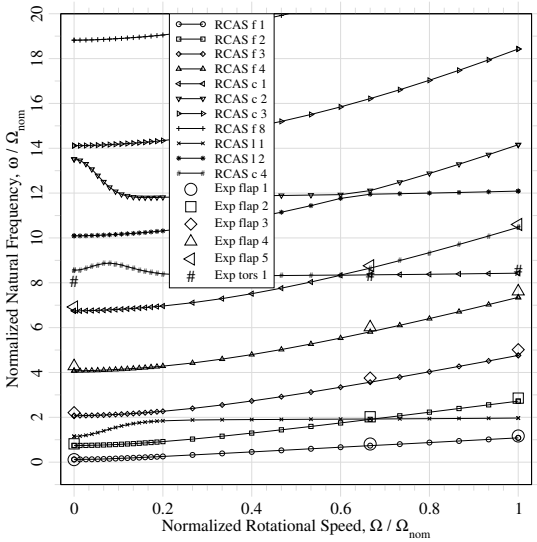

Figure 20: Swept tip natural frequencies: experiment vs. RCAS for $N = 17$ and $\Lambda = 0°$ with gravity.

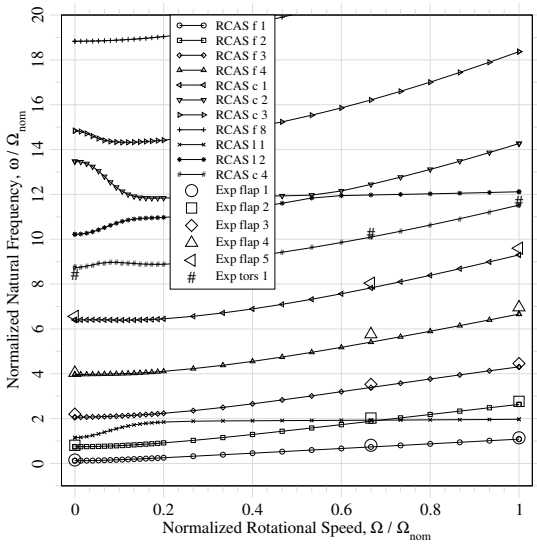

Figure 21: Swept tip natural frequencies: experiment vs. RCAS for $N = 17$ and $\Lambda = 15°$ with gravity.

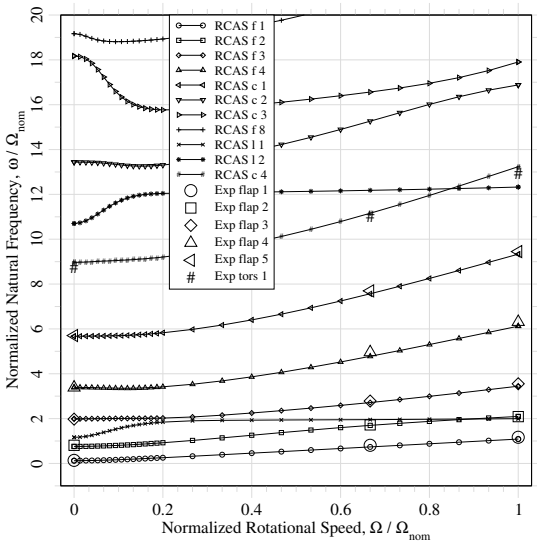

Figure 22: Swept tip natural frequencies: experiment vs. RCAS for $N = 17$ and $\Lambda = 45°$ with gravity.

as evident in the "Princeton Beam" analysis, the edgewise frequencies are significantly influenced by the static deflection induced coupling of the edgewise and torsion motion. The effects of gravity were not included in the analytical results of references [25, 26], however, this did not affect the analytical experimental comparisons since only flapwise and torsion mode experimental measurements were obtained. As a result, the predominant effects of gravity cannot not be compared with the present calculations.

A more subtle effect of gravity is the coupling of torsion with the fifth flap mode. On the left side of Fig. 20, c1 is the fifth flap mode and c4 is the first torsion mode, but on the right side the roles are reversed. The curves which crossed in Fig. 18 only closely approach each other in Fig. 20. A similar interaction occurs between the second lag mode and the sixth flap mode. (However the coupled lag mode will still be labeled l2 to facilitate focusing on flap coupling.)

With the introduction of a $\Lambda = 15°$ sweep angle the frequency as a function of rotor speed is presented in Fig. 21. The first torsion mode is strongly affected. The mode labeled c1, is returning to the characteristics of a fifth flap mode. The modes labeled c2 and c4 are coupled torsion and sixth flap modes with some coupling to l1, the lag mode.

At the maximum experimental sweep angle, $\Lambda = 45°$, (Fig. 22) illustrates the frequencies behavior with respect to rotor speed. The mode c4 is taking on more of the characteristics of the sixth flap mode (especially at higher rotor speeds). The modes c2 and c3 are coupled first torsion and seventh flap modes.

With the addition of a plot of modal frequency vs. sweep angle at the nominal rotor speed, Ω_{nom} (Fig. 23) in conjunction with Fig. 22, Fig. 19, and Fig. 20, it is possible to trace each eigenvalue around a closed circuit and insure consistent identification. The evolution of the torsion mode as it couples successively with the fifth, sixth, and seventh flap modes is readily apparent in Fig. 23 The experimental frequency measurements reflect only the first six flap modes, that is, the torsion mode frequency for 45 deg sweep angle was above the range of the measurements (and the reported measurement was most likely the sixth flap mode. These observations differ in some respects from the designation of modes given in references [25, 26].

The comparisons indicate that RCAS correctly models the effects of sweep angle on the rotating blade coupled flap and torsion frequencies.

Hinged Rotating Beam Comparisons

As noted in Aeroelasticity [27] and other texts, the eigensolutions for a rotating beam, pinned at the axis of rotation, can be analytically represented in series form using Duncan polynomials. Harris [28], by specifying a

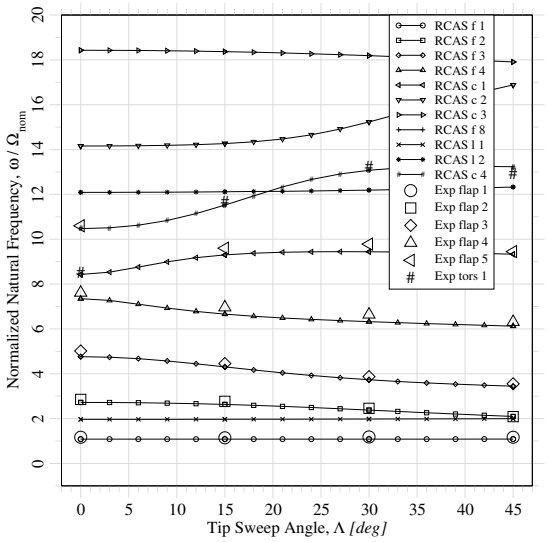

Figure 23: Swept tip natural frequencies: experiment vs. RCAS for $N = 17$ and $\Omega = \Omega_{nom}$ with gravity.

solution with a finite number of rational coefficients, defined a problem with that exact solution. He proposed that problem be used as an analytical test case for validating finite element computer programs. The relevant parameters for the eigenvalue problem are $R = 28$ ft, $\Omega = V_{tip}/R = 650/28$ rad/sec, $EI = 5R^3 = 109,760$ lb-ft^2, and $m = 168/845$ slug/ft. The corresponding dimensionless reference frequency parameter ([27]) is $1/K = m\Omega^2 R^4/EI = 1/600$. Solution of the transcendental equation associated with the analytical problem, retaining the first 70 terms in the series, has been carried out by the author of the problem ([28]) and made available through a personal communication [29].

RCAS models were developed with $N = 10$ and $N = 20$ elements. Motion was restricted to flap displacement and rotation. The root was hinged at the rotational axis. A comparison of the RCAS and analytical results [29] is presented in Table 2.

As anticipated, errors (assuming the analytical solution is exact) using finite elements are consistently small and decrease when more elements are used. For the second mode, the error was 0.005% for $N = 10$ and .001% for $N = 20$. For the tenth mode, the error was 2% for $N = 10$ and 0.2% for $N = 20$.

Natural Frequencies Rotating, Pinned-Free Beam			
Mode	RCAS N=10	RCAS N=20	Analytical
1	0.999999	0.999999	1.0
2	2.55726	2.55714	2.55711
3	4.58062	4.58006	4.57997
4	7.24717	7.24458	7.24431
5	10.5852	10.5742	10.5733
6	14.6469	14.6097	14.6067
7	19.4912	19.3883	19.3798
8	25.1758	24.9371	24.9164
9	31.7440	31.2763	31.2299
10	39.1465	38.4232	38.3444

Table 2: Hinged rotating beam natural frequencies: analytical [29] vs. RCAS for $N = 10$ and $N = 20$ element models.

Periodic Boundary Load Problems

One problems tested the work terms associated with time varying boundary loading. The flight-test loads of a real world, full scale, UH-60 aircraft rotor blade experiencing periodic loading, during steady level flight.

UH-60 Blade Loads

The prediction of rotor blade loads in response to unsteady aerodynamic forces is one of the most difficult problems in rotorcraft analysis. For most flight conditions, complex fluid flow phenomena prevent aerodynamic lift, drag, and moments from being calculated accurately enough to determine the dynamic response and structural loads of the rotor blades with accuracy needed for design purposes. Even if accurate aerodynamic analyses were available, the complex structural dynamics of a nonuniform, flexible, rotating beam remains a very daunting problem with little evidence to demonstrate that accurate solutions can be achieved with current analysis methods. This problem involves dynamic coupling of the fuselage, rotor, controls, and engine drive train components. The blades involve large rigid body pitch, flap, and lead-lag rotations, as well as significant elastic deformations in flapwise, chordwise bending, and torsion. The large rigid body blade rotations involve nonlinear kinematic effects and the blade elastic deflections involve nonlinear coupling of bending and torsion motions. Therefore, the full problem involves many complicated dynamic and structural dynamics effects.

The present problem affords gaining insight into the accuracy of rotor blade structural dynamics analysis by

applying experimentally measured airloads to a rotor blade model and comparing the resulting blade loads with corresponding experimental blade loads. This opportunity is available as a result of the full-scale flight test investigation of the NASA/Army UH-60 Airloads Program reported in [30]. An extensively instrumented UH-60 aircraft was used to comprehensively measure, among other things, blade motion, surface pressures, and structural blade loads for a variety of flight conditions. The present problem describes the initial results of an investigation to apply the RCAS computer program to calculate rotor blade loads in response to the measured airloads and in turn compare the calculated blade loads with the corresponding measured loads. In this way the accuracy of the structural dynamics analysis may be assessed without the necessity of dealing with aerodynamics analysis issues.

Of course, aside from the analysis itself, the results are subject to the accuracy of the experimentally measured airloads and blade loads as well as the accuracy of the physical properties of the blade structure. Other important considerations for this problem include choices for modeling the actual physical structure, the choice of degrees of freedom are to be included or excluded, and how to properly represent the boundary conditions to define a well posed problem. In addition, some consideration must also be given to the numerical solution procedures to insure convergence and practical computations. The generality of the RCAS computer program provides opportunities for developing complex structural models and applying various solution methodologies tailored to the problem at hand. The following discussion will briefly survey the approach used for this problem.

For this initial investigation, several assumptions were made to bound the scope of the problem. First, the problem was limited to a single isolated rotor blade rotating with constant angular velocity about a point traveling in a straight line with constant velocity. That is, any dynamic effects of fuselage or engine drive train coupling with the rotor are ignored including any coupling between blades through swashplate flexibility.

The RCAS structural model is schematically depicted in Fig. 24 and is composed of a series of elements including rigid bars, linear rotational and translational springs and dampers, a rigid body mass, hinges, a slide, and twelve nonlinear beam finite elements. The outboard tip of the blade is swept, the structural and aerodynamic axes of the blade are twisted non-uniformly along the radius, a series of rigid bars and spring elements are used to represent the pitch control linkage and a slide element is introduced to control blade collective and cyclic pitch inputs. A linear lag damper element is provided, however, for the results presented, the actual measured damper force

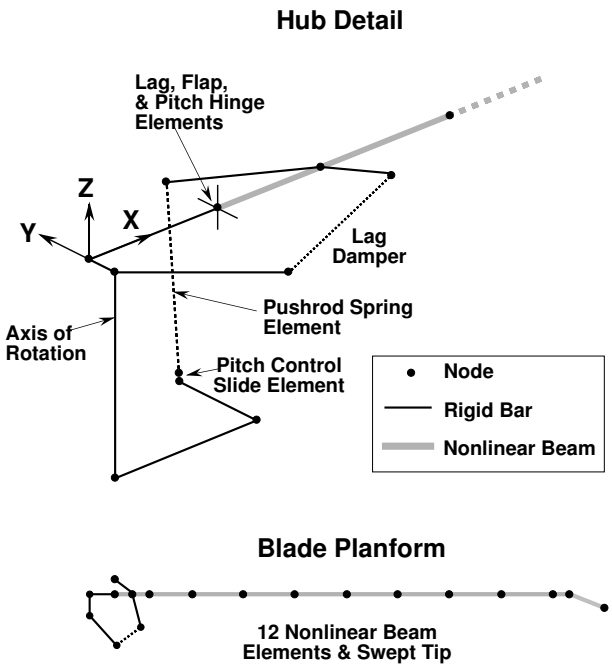

Figure 24: UH-60 rotor blade structural model schematic.

is used as a blade excitation because the actual physical damper characteristics are highly nonlinear. The blade root hinge is offset from the center of rotation and the actual elastomeric bearing which accommodates simultaneous rotations in all three axes is represented by three discrete coincident hinge elements for flap, lag, and pitch rotation of the blade. Physical properties for all of the elements of the blade model were included as appropriate.

To introduce the aerodynamic normal force, chord force, and pitching moment, the measured blade surface pressures were integrated at nine radial locations to obtain the forces and moments per unit length, and these were interpolated and applied as discrete forces and moments, referred to as mechanical applied loads, at 27 locations distributed along the blade. The loads were applied in the appropriate airfoil chord coordinates and followed the blade orientation as it underwent rigid flap, lead-lag, and pitch motions as well as elastic bending and torsion deformations. Similarly, the blade loads, flapwise bending, chordwise bending and torsion moments were calculated in the local deformed blade coordinate systems.

For the solution process, the periodic mechanical applied loads representing aerodynamic and lead-lag damper were applied to the rotating blade structure and the solution proceeded either in 1) the time domain using a time integration procedure until a converged periodic

solution for the system degrees of freedom was obtained or, 2) a frequency domain solution procedure was applied based on an assumed harmonic solution. The later procedure was most commonly applied as the number of harmonics of the solution could be conveniently specified and this automatically filtered high frequency noise from the experimental airloads data. Ten harmonics were retained for the results presented. To facilitate numerical convergence of the solutions, structural damping was used to damp initial transients and then withdrawn as a function of time as the solution converged. In addition to the small discrete dampers used to represent the blade root hinge elastomeric bearing, 0.02% structural damping was introduced into the elastic blade structure.

Representing aerodynamic forces as fixed mechanical loads, rather than being motion dependent as in typical coupled aeroelastic blade loads analyses, eliminates the inherent aerodynamic damping that typically aids the numerical solution convergence of aeroelastic analyses. For the present purely structural dynamic response analysis, the absence of damping can present numerical convergence problems, thus necessitating the approach adopted herein. For cases with very small dampers or structural damping, problems may arise if system natural frequencies fall close to the N/rev excitation frequencies. For example, the rigid flap natural frequency of an articulated blade with zero hinge offset is 1.0/rev and, if there is no damper, response will be infinite if the flapping moment excitation is not zero. In such a case, the 1/rev aerodynamic flap moments must be identically zero and this is consistent with the observed finite flapping response of actual blades with zero hinge offset. However, if experimentally measured airloads contain any small errors, the calculated dynamic response would be infinite. This simply reflects the fact that calculating dynamic response from experimentally measured airloads will be impossible or impractical if system natural frequencies of modes with very small damping are too close to N/rev excitations. In the present case, the rigid flap mode frequency is approximately 1.035/rev and this is sufficiently far from 1/rev to enable reasonably accurate flap motion response to be calculated, even though the 1/rev aerodynamic flap moment is very small.

Typical results for blade loads are given in Fig. 24 - Fig. 28 for the blade flapwise and edgewise bending moments and torsion moment at several radial stations as a function of blade azimuth.

The flight condition for these results is level flight at 0.368 advance ratio. Calculated flapwise bending moments at 50% blade radius are compared with experimental measurements in Fig. 25 and the results are shown to be reasonable. Chordwise bending moments are com-

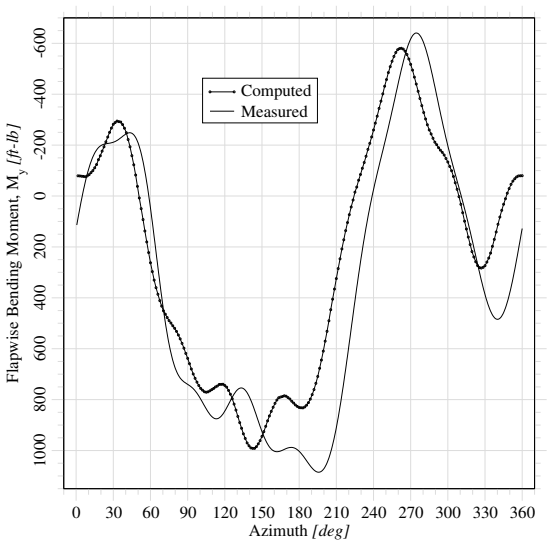

Figure 25: UH-60 blade flapwise bending moment, 30% R. Calculated blade loads, measured blade loads.

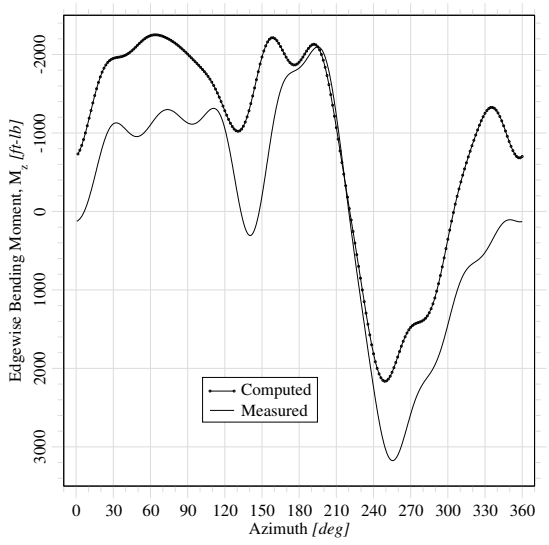

Figure 26: UH-60 blade edgewise bending moment, 11.3% R.

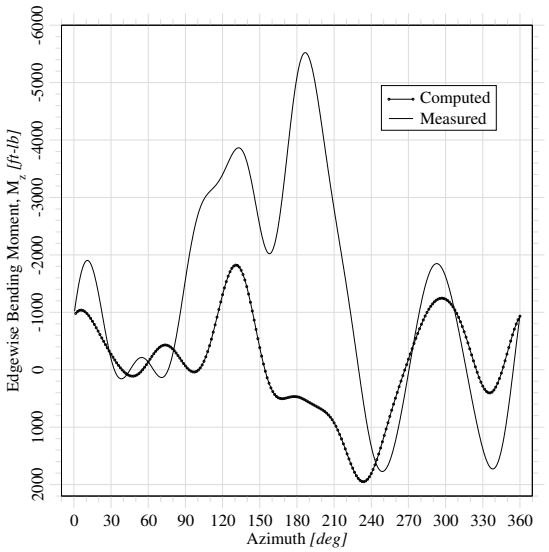

Figure 27: UH-60 blade edgewise bending moment, 50% R.

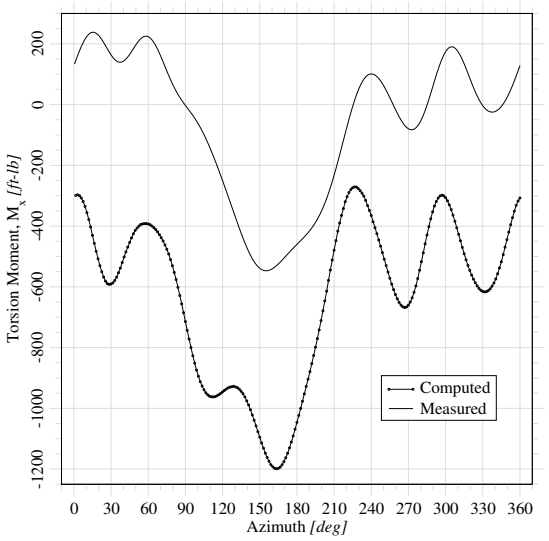

Figure 28: UH-60 blade torsion moment, 30% R.

pared for two radial stations in Figs. 26 and 27. For the 11.3% inboard station, the results are in good agreement, reflecting the effective constraint of the lead-lag damper force applied at the adjacent damper attachment location at 8.1% blade radius. At the 50% radial station the agreement is only fair, as the measured peak bending moment response is not captured by the calculated result. It is hypothesized that this may be related to the constant rotor speed assumption in the analysis. A comparison of torsion moments at the 30% blade radius is given in Fig. 28 and the results are in good agreement as far as the oscillatory behavior is concerned. There is a significant difference in the mean values of the torsion moment that may be due to experimental measurement error.

The present results have been calculated assuming the boundary conditions for the blade flap and lag motion are free motion at the blade root hinge. The blade root pitch motion (collective and cyclic) was input at the controlled slide element at the base of the pushrod. Strictly speaking, this pitch control input must be adjusted on subsequent iterations to account for the pushrod elastic deflections in order to match the measured blade pitch input. An alternative approach would be to use the measured blade pitch and lag hinge motion as prescribed boundary conditions for calculating the blade load response. To conclude, the initial results presented here are encouraging and provide a measure of confidence in the capabilities of an advanced structural dynamics computer program when applied to a typically complex real-world rotor blade configuration.

Conclusions

The hybrid element addressing both rigid and flexible body kinematics has been shown to be effective. The RCAS implementation of the element is consistent with expectations for the cases investigated. Error predictions for the element correlate well with results. An assemblage of elements each with moderate deformations can accommodate large rigid body motions and deformations. The tests exercising static energy, fixed frame kinetic energy, rotating frame kinetic energy, and periodic boundary work produce consistent results.

Furthermore, the combination of improved finite element methods and novel approaches for eliminating systematic discrepancies has resulted in significant correlation improvements with benchmark analytical and experimental data. The RCAS nonlinear beam element formulation is shown to be adequate for beam elastic deformations beyond the range necessary for rotorcraft applications. The code is shown to be applicable for complex

rotor blade configurations as well.

Acknowledgments

The authors gratefully acknowledge the contributions of Dr. Hossein Saberi, Vice President of Engineering, Advanced Rotorcraft Technology, Inc., for advancements leading to the development of RCAS as well as considerable effort to facilitate generation of results presented in the paper.

References

[1] Peter W. Likins. Dynamics Analysis of a System of Hinge-Connected Rigid Bodies with Nonrigid Appendages. Technical Report 32-1576, Jet Propulsion Laboratory, California Institute of Technology, Pasadena, California, February 1974.

[2] Arthur Stewart Hopkins. The Motion of Interconnected Flexible Bodies. Technical Report UCLA-ENG-7513, School of Engineering and Applied Science, University of California, Los Angeles, California, February 1975.

[3] A. Stewart Hopkins and Donald L. Kunz. General Rotorcraft Aeromechanical Stability Program (GRASP) Version 1.03—User's Manual. NASA Technical Memorandum 100043, Aeroflightdynamics Directorate, U. S. Army Aviation Research and Technology Activity, Moffett Field, California, February 1988.

[4] Dewey H. Hodges, A. Stewart Hopkins, Donald L. Kunz, and Howard E. Hinnant. General Rotorcraft Aeromechanical Stability Program (GRASP) Theory Manual. NASA Technical Memorandum 102255, Aeroflightdynamics Directorate, U. S. Army Aviation Research and Technology Activity, Moffett Field, California, October 1990.

[5] Anon. 2GCHAS Applications Manual, Version 2.4. USAATCOM Technical Memorandum 93-A-001, US Army Aviation and Troop Command, Moffett Field, CA, August 1995.

[6] Anon. 2GCHAS Programer's Manual, Version 2.2. USAATCOM Technical Memorandum 93-A-003, US Army Aviation and Troop Command, Moffett Field, CA, July 1993.

[7] Anon. 2GCHAS Theory Manual, Version 3.0. USAATCOM Technical Memorandum 93-A-004, US Army Aviation and Troop Command, Moffett Field, CA, March 2001.

[8] Anon. 2GCHAS User's Manual, Version 2.4. USAATCOM Technical Memorandum 93-A-002, US Army Aviation and Troop Command, Moffett Field, CA, August 1995.

[9] Anon. RCAS Theory Manual, Version 2.0. Technical Report USAAMCOM/AFDD TR 02-A-005, US Army Aviation and Missile Command, Moffett Field, CA, June 2002.

[10] Anon. RCAS User's Manual, Version 2.0. Technical Report USAAMCOM/AFDD TR 02-A-006, US Army Aviation and Missile Command, Moffett Field, CA, June 2002.

[11] Anon. RCAS Applications Manual, Version 2.0. Technical Report USAAMCOM/AFDD TR 02-A-007, US Army Aviation and Missile Command, Moffett Field, CA, June 2002.

[12] Hossein-Ali Saberi, Yoon C. Jung, and Tassos Anastassiades. Finite Element and Modal Method in Multibody Dynamic Code. In *American Helicopter Society, Northeast Region, 2nd International Aeromechanics Specialists' Conference Proceedings*, volume I, Bridgeport, Connecticut, October 1995.

[13] D. H. Hodges and E. H. Dowell. Nonlinear Equations of Motion for the Elastic Bending and Torsion of Twisted Nonuniform Rotor Blades. Technical Note NASA TN D-7818, NASA, Washington, DC, December 1974.

[14] Stephen P. Timoshenko and James M. Gere. *Mechanics of Materials*. D. Van Nostrand Company, New York, 1972.

[15] E. H. Dowell, J. Traybar, and Dewey H. Hodges. An Experimental Theoretical Correlation Study of Non-Linear Bending and Torsion Deformations of a Cantilever Beam. *Journal of Sound and Vibration*, 50(4):533–544, February 1977.

[16] Joon W. Lim and T. Anastassiades. Correlation of 2GCHAS Analysis with Experimental Data. *Journal of the American Helicopter Society*, 40(4), October 1995.

[17] A. Rosen and P. Friedmann. The Nonlinear Behavior of Elastic Slender Straight Beams Undergoing Small Strains and Moderate Rotations. *Journal of Applied Mechanics*, 46:161–168, March 1979.

[18] E. H. Dowell and J. Traybar. An Experimental Study of the Nonlinear Stiffness of a Rotor Blade Undergoing Flap, Lag and Twist Deformations. AMS Report No. 1194, Princeton University, January 1975.

[19] E. H. Dowell and J. J. Traybar. An Addendum to AMS Report No. 1194 Entitled An Experimental Study of the Nonlinear Stiffness of a Rotor Blade Undergoing Flap, Lag and Twist Deformations. AMS Report No. 1257, Princeton University, December 1975.

[20] ASM International Handbook Committee, editor. *Properties and Selection: Nonferrous Alloys and Special-Purpose Materials*, volume 2 of *Metals Handbook*, chapter Specific Metals and Alloys, pages 115–116. ASM International, tenth edition, 1990.

[21] George W. Housner and Jr. Thad Vreeland. *The Analysis of Stress and Deformation*. The Macmillan Company, New York, 1966.

[22] S. P. Timoshenko and J. N. Goodier. *Theory of Elasticity*. McGraw-Hill, Inc., New York, Third edition, 1970.

[23] Walter C. Hurty and Moshe F. Rubinstein. *Dynamics of Structures*. Prentice-Hall, Inc., Englewood Cliffs, New Jersey, 1964.

[24] Roberto Celi and Peretz P. Friedmann. Aeroelastic Modeling of Swept Tip Rotor Blades Using Finite Elements. *Journal of the American Helicopter Society*, 33(2):43–52, April 1988.

[25] Jeanette J. Epps and Ramesh Chandra. The Natural Frequencies of Rotating Composite Beams With Tip Sweep. *Journal of the American Helicopter Society*, 41(1):29–36, January 1996.

[26] Dewey H. Hodges, Xiaoyang Shang, and Carlos E. S. Cesnik. Finite Element Solutions of Nonlinear Intrinsic Equations for Curved Composite Beams. *Journal of the American Helicopter Society*, 41(4):313–321, October 1996.

[27] Raymond L. Bisplinghoff, Holt Ashley, and Robert L. Halfman. *Aeroelasticity*. Dover Publications, Inc., Mineola, NY, 1996.

[28] Franklin D. Harris. The Rotor Blade Flap Bending Problem — An Analytical Test Case. *Journal of the American Helicopter Society*, 37(4):64–67, October 1992.

[29] Franklin D. Harris. Normal Modes Solution To The Rotor Flap Bending Problem Posed in the Journal of the AHS (Vol. 37, No. 4, Oct. 1992). Personal Communication, February 2003.

[30] Robert M. Kufeld, Dwight L. Balough, Jeffrey L. Cross, Karen F. Studebaker, Christopher D. Jennison, and William G. Bousman. Flight Testing the UH-60A Airloads Aircraft. In *American Helicopter Society 50th Annual Forum Proceedings*, volume I, Washington, DC, May 1994.